Mind Your Clever Neighbours: Unsupervised Person Re-identification via Adaptive Clustering Relationship Modeling

Lianjie Jia[1,*], **Chenyang Yu**[2,*], **Xiehao Ye**[1], **Tianyu Yan**[1], **Yinjie Lei**[3], **Pingping Zhang**[1†]
[1]**School of Artificial Intelligence, Dalian University of Technology**
[2]**School of Information and Communication Engineering, Dalian University of Technology**
[3]**College of Electronics and Information Engineering, Sichuan University**
{banana,yuchenyang,1617464594,2981431354}@mail.dlut.edu.cn, {yinjie}@scu.edu.cn,
{zhpp}@dlut.edu.cn

Abstract

Unsupervised person re-identification (Re-ID) attracts increasing attention due to its potential to resolve the scalability problem of supervised Re-ID models. Most existing unsupervised methods adopt an iterative clustering mechanism, where the network was trained based on pseudo labels generated by unsupervised clustering. However, clustering errors are inevitable. To generate high-quality pseudo-labels and mitigate the impact of clustering errors, we propose a novel clustering relationship modeling framework for unsupervised person Re-ID. Specifically, before clustering, the relation between unlabeled images is explored based on a graph correlation learning (GCL) module and the refined features are then used for clustering to generate high-quality pseudo-labels. Thus, GCL adaptively mines the relationship between samples in a mini-batch to reduce the impact of abnormal clustering when training. To train the network more effectively, we further propose a selective contrastive learning (SCL) method with a selective memory bank update policy. Extensive experiments demonstrate that our method shows much better results than most state-of-the-art unsupervised methods on Market1501, DukeMTMC-reID and MSMT17 datasets. We will release the code for model reproduction.

Introduction

Person re-identification (Re-ID) (Chen et al. 2019a) aims at searching the same person among images captured by non-overlapping cameras. In recent years, this task has drawn increasing attention due to its potential applications such as person searching (Loy, Xiang, and Gong 2009) and object tracking (Yan et al. 2020). Previous approaches (Liu et al. 2015; Xu et al. 2017; Liu et al. 2021) mostly focus on supervised Re-ID, which uses human-annotated labels to build discriminative representations. However, it is both time consuming and labour cost to annotate cross-camera identity labels. To overcome these challenges, increasing efforts have been shifted to unsupervised person Re-ID, which directly builds a model with unlabeled data.

Depending on whether using extra labeled data, existing unsupervised person Re-ID methods (Wang and Zhang 2020; Jin et al. 2020; Fu et al. 2019) can be divided into two categories, *i.e.*, unsuperivsed domain adaptation (UDA) and purely unsupervised learning (USL). The main idea of UDA is to adjust a model from a labeled source dataset to an unlabeled target dataset. Thanks to the introduction of large-scale annotated source datasets, state-of-the-art UDA methods (Lin et al. 2018; Deng et al. 2018; Zhai et al. 2020) significantly enhance the performance of unsupervised Re-ID. However, the success of such system relies on the assumption that the difference between the source domain and target domain is not significant. Meanwhile the training procedure for UDA is complex. In contrast, USL does not require any identity annotations and directly learns from unlabeled data in the target dataset, thus shows better flexibility.

Existing USL methods (Lin et al. 2019; Dai et al. 2021; Zhang et al. 2021) mainly adopt an iterative clustering mechanism, where the network is trained based on pseudo la-

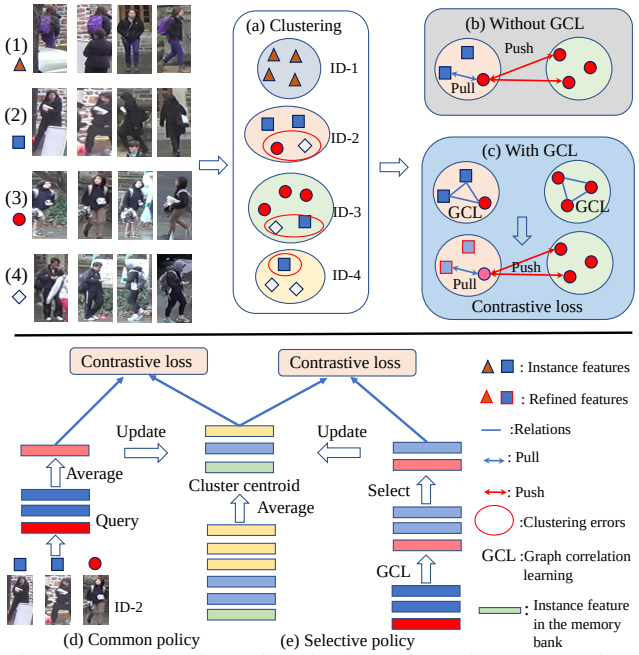

Figure 1: Illustration of typical problems in unsupervised person Re-ID. (a) Appeared clustering errors; (b) Methods trained without GCL module; (c) Methods trained with GCL module; (d) Common policy in memory bank updating; (e) Our selective policy.

.

*Equal Contributions
†Corresponding Author

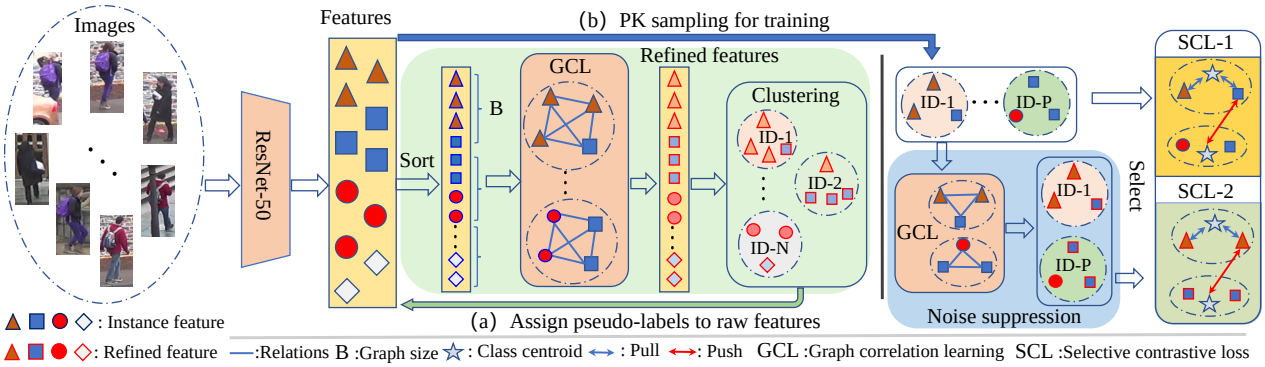

Figure 2: Illustration of the proposed framework. (a) Unlabeled data are first represented by feature vectors through ResNet-50 (He et al. 2016). The graph correlation learning (GCL) module is designed to explore the relationship of sorted unlabeled examples, and the raw features are assigned to pseudo labels by a typical clustering algorithm with the refined features. (b) Once the pseudo labels are captured, we conduct PK sampling (Hermans, Beyer, and Leibe 2017) for training. And the GCL is used to suppress noisy samples in a mini-batch to reduce the impact of clustering errors. Finally, the selective contrastive loss (SCL) is used to train the model.

bels generated by unsupervised clustering. However, previous methods have not considered the relationship between samples before clustering, leading to sub-optimal clustering results. To solve this problem, we propose a new unsupervised Re-ID framework with a graph correlation learning (GCL) module. Instead of directly using the output of a feature extractor for clustering, we first model the relationship between samples in the training dataset. Since it is very expensive to build a graph for the entire dataset, we construct a series of small graphs in a batch size. What's more, in typically unsupervised person Re-ID, clustering errors are inevitable. As shown in Fig.1 (a) and (b), because a pseudo-label is usually composed of multiple instances, it hurts the Re-ID performance when images of different identities are considered as the same class. In this work, the proposed GCL module is used to reconstruct the representation of samples in a mini-batch, as shown in Fig.1 (c). In this way, we not only improve the quality of clustering, but also alleviate the impact of clustering errors.

Meanwhile, the construction of a memory bank is also critical for contrastive learning (Tian et al. 2020). As shown in Fig.1 (d), a typical method (Ge et al. 2020) is to store the feature vector of every instance inside the memory dictionary and compute the contrastive loss with the query instance. Since the clustering approach (Ester et al. 1996) inevitably introduces noisy samples, the average operation for the memory bank would contaminate its corresponding cluster feature representation. As shown in Fig.1 (e), to alleviate this problem, we propose a novel selective contrastive learning (SCL) method with a dynamic class-level memory bank. Specifically, once we get the pseudo-labels of the training set, we first select the averaged feature of all samples belonging to the class to initialize the class centroid in the memory bank. Then, according to the defined distance metric, we rank the similarity order between the query instance feature and the class centroid. Top-k dissimilar query instances in a mini-batch will be selected to update the memory bank. Extensive experiments on three benchmarks show the effectiveness of our method.

Our main contributions can be summarized as follows:

- We propose a graph correlation learning (GCL) module to improve the quality of clustering, considering the relationship between examples and its neighbors.
- We propose a novel selective contrastive learning (SCL) method, in which top-k dissimilar query instances in a mini-batch will be selected to update the memory bank.
- Extensive experiments demonstrate that our proposed method outperforms existing state-of-the-art unsupervised methods on three large-scale datasets, *i.e.*, Market-1501, DukeMTMC-reID and MSMT17.

Related Work

Unsupervised person Re-ID aims to build a Re-ID model with only unlabeld data. Thus, this work is closely related to contrastive learning methods with clustering.

Memory bank based contrastive learning methods, such as MoCo (He et al. 2020), InfoMin (Tian et al. 2020) and SimCLR (Chen et al. 2020), have been widely used for different vision tasks. These methods generate positive samples using data augmentation, then the representation is learned by a non-parameter contrastive loss (Wu and Wang 2021). However, if samples in the dataset are highly correlated, *e.g.*, specific pedestrian under different cameras in Re-ID task, the training process of contrastive learning will be unreliable. The reason is that the negative samples are likely to be composed of highly similar instances (actually samples with the same identity). One solution for unsupervised person Re-ID (Pang et al. 2020) is to cluster the instances first, so that similar instances are grouped into the same class; and then perform contrastive learning, thereby alleviating the false rejection of high-similarity instances.

Recently, most pseudo-label based unsupervised person Re-ID methods (Chen, Lagadec, and Bremond 2021; Lin et al. 2020; Yin et al. 2021) try to improve performance from the following three aspects: (1) high-quality pseudo label generation; (2) effective memory bank initialization and update; (3) appropriate model training. Specifically, Lin *et*

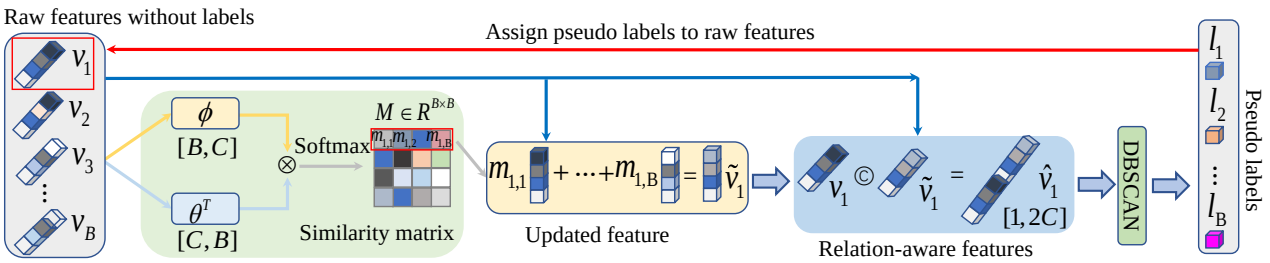

Figure 3: Illustration of the proposed cluster refinement based on graph correlation learning.

al.(Lin et al. 2019) proposed a bottom-up clustering framework that iteratively trains a network based on the pseudo labels. Wang *et al.*(Wang et al. 2019) formulated unsupervised person Re-ID as a multi-label classification task and used a memory bank to train the network. Wang *et al.*(Wang et al. 2021) calculated identity centroids for each camera and conducted intra-and inter-camera centroid contrastive learning. Although these methods have achieved great success, they rely on the accuracy of pseudo labels. Intuitively, high-quality clustering results will improve the performance of these models. Zhang *et al.*(Zhang et al. 2021) first estimated pseudo label similarities and then refined pseudo labels with temporally propagated and aggregated soft labels. Instead of directly optimizing pseudo-labels, we optimize the features used by clustering with a non-parameter GCL module, thereby potentially obtaining high-quality pseudo-labels. Dai *et al.*(Dai et al. 2021) proposed to select the hardest query feature from a mini-batch to update the cluster feature. However, since the clustering approach inevitably introduces noisy samples, the hardest samples in a mini-batch are likely to be outliers. To alleviate the above problem, we use GCL to reduce the impact of abnormal clustering when training, and propose a novel SCL method with a selective memory bank updating policy.

Proposed Method

As illustrated in Fig.2, the proposed framework mainly includes three components: (1) Before clustering, the relationship between unlabeled examples is explored by the GCL module and the refined features are then used for clustering to generate high-quality pseudo-labels. (2) After clustering, we use pseudo-labels to train the model. In order to reduce the impact of clustering errors, we use GCL to mine the relationship between samples in a mini-batch. (3) The SCL is used to train the model, which pulls positive pairs together and repels negative pairs.

Graph Correlation Learning for Clustering

Given a training set of human images $\{I_i\}_{i=1}^N$, where I_i is an image without labels, they are first represented by feature vectors $F = \{f_i\}_{i=1}^N$ through ResNet-50 (He et al. 2016), where $f_i \in R^{C\times H\times W}$, in which C, H, W represent the channel, height and width, respectively. We then sequentially utilize a global average pooling (GAP) to obtain the image-level representation $v_i \in R^{1\times C}$.

When performing unsupervised clustering, it is necessary to traverse the entire training set in a certain order (Lin et al. 2019). In practice, it is a common way to sort the training set according to the image name. There is such a prior knowledge in the Re-ID task that if we sort the training set, the images with the same identity will gather together. With the representations $V = \{v_i\}_{i=1}^N$ of the entire training set, we sort V according to the image names. We then preprocess the representations by GCL to improve the clustering result, as shown in Fig. 3.

At first, we divide the representation of sorted training set $V = \{v_i\}_{i=1}^N$ into small graphs $G = [\{v_i\}_{i=1}^B, \ldots, \{v_i\}_{i=n*B+1}^N]$, where B is the number of images in a graph and n is the number of graphs. Without the loss of generality, we choose samples in the first graph $\{v_i\}_{i=1}^B$ in G as an example. Let $\mathcal{G}(\mathcal{V}, \mathcal{E})$ be the constructed graph of B nodes with nodes $v_i \in \mathcal{V} \subset V$ and edges $e_{ij} = (v_i, v_j) \in \mathcal{E}$. The edge e_{ij} represents the relation between the i^{th} node and the j^{th} node. Termed the B feature nodes as $v_i \in R^{1\times C}$, where $i = 1, 2, \ldots, B$. The pairwise relation m_{ij} from node i to node j can be defined as

$$m_{ij} = e(v_i, v_j) = \theta(v_i)^T \phi(v_j) \tag{1}$$

where θ and ϕ are embedding functions. In practice, θ and ϕ can be implemented by a fully connected layer followed by a batch normalization (BN) (Ioffe and Szegedy 2015) and L2 normalization, *i.e.*, $\theta(v_i) = Norm(BN(W_\theta v_i))$ and $\phi(v_j) = Norm(BN(W_\phi v_j))$. The learnable parameter W_θ and W_ϕ are $C \times C$ dimension weight matrices. Inspired by (Li et al. 2018), we convert the relations between any two nodes into attention scores by

$$m_{ij} = \frac{\exp(e(v_i, v_j) * T)}{\sum_{k=1}^B \exp(e(v_i, v_k) * T)} \tag{2}$$

where T is a temperature parameter. Once the attention scores m_{ij} between nodes are obtained, we can update the node features as

$$\widetilde{v_i} = \sum_{j=1}^{B} m_{ij} v_j \tag{3}$$

where $\widetilde{v_i}$ represents the refined node feature. Then we concatenate the raw node feature v_i and the updated node feature $\widetilde{v_i}$ to get the relation-aware node feature

$$\hat{v_i} = [v_i, \widetilde{v_i}]. \tag{4}$$

Finally, instead of the raw node features, the relation-aware node features $\hat{V} = \{\hat{v_i}\}_{i=1}^N$ are used to generate the pseudo-labels $L = \{l_i\}_{i=1}^N$ through DBSCAN (Ester et al.

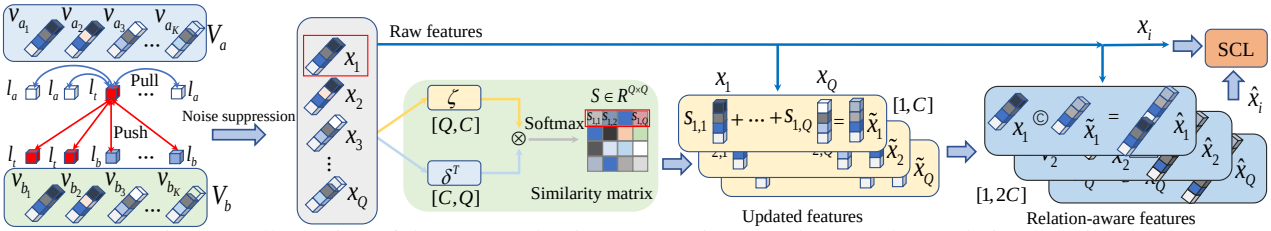

Figure 4: Illustration of the proposed noise suppression based on graph correlation learning.

1996). Since $\hat{V}$ contains certain structural information in neighbour, it can potentially make the features of the same identity close to each other. As a result, better clustering results can be obtained. Thanks to the one-to-one correspondence between $\hat{V}$ and images I, we can assign corresponding pseudo labels to I. Through above steps, we have completed the refinement of the clustering.

Noise Suppression

After clustering, an unsupervised training set is transformed into a supervised training set $\{I_i, L_i\}_{i=1}^{N}$, where I_i is an image with the label $L_i \in \{0, 1, \ldots, len(L)\}$ and $len(L)$ represents the total number of clusters. During training, we randomly sample P person identities for each mini-batch. Meanwhile we randomly select K instances for each person. All the $P \times K$ images are fed into the feature extractor to get the frame-level representations $V_{PK} = \{v_i\}_{i=1}^{P \times K}$. Then the instance contrastive loss can be used to pull positive pairs together and repel negative pairs in the embedding space.

As shown in Fig. 4, there are two selected persons, corresponding to pseudo-labels l_a and l_b respectively. Since the clustering approach inevitably introduces noisy samples, there will be some noise samples in the selected persons, whose true label should be l_t. Termed the instance representations of two selected persons as $V_a = \{v_{a_1}^{l_a}, v_{a_2}^{l_a}, \ldots, v_{a_K}^{l_a}\}$ and $V_b = \{v_{b_1}^{l_t}, v_{b_2}^{l_t}, \ldots, v_{b_K}^{l_b}\}$, where superscript l represents the true label of the instance and subscript a_i and b_i represent the index of the sampling instance. Thanks to the contrastive loss, the noise sample $v_{a_3}^{l_t}$ will be pulled in with $v_{a_1}^{l_a}$ and will be moved away from $v_{b_1}^{l_t}$ and $v_{b_2}^{l_t}$. Obviously, this unreasonable operation will affect the learning of the network. To alleviate the above problem, the proposed GCL module is used to reconstruct the representation of samples in a mini-batch when training.

More specifically, we take the image-level representations as the graph nodes. All the $Q = P \times K$ samples in a mini-batch form a graph G with Q nodes. We represent the feature nodes as $x_i \in R^{1 \times C}$, where $i = 1, 2, \ldots, Q$. Similar to GCL used to refine clustering results, the pairwise relation s_{ij} from node i to node j can be defined as follows

$$s_{ij} = e(x_i, x_j) = \delta(x_i)^T \zeta(x_j) \tag{5}$$

where δ and ζ are embedding functions implemented by a fully connected layer followed by batch normalization (BN) and L2 normalization, *i.e.*, $\delta(x_i) = Norm(BN(W_\delta x_i))$ and $\zeta(x_j) = Norm(BN(W_\zeta x_j))$. It is worth noting that the learnable parameters W_δ and W_ζ share the same weight matrix with W_θ and W_ϕ, respectively. In this way, the GCL module used to refine the clustering results can also be trained end-to-end. Similar to Eq.(2), we can represent the pairwise relations for all the nodes in a mini-batch by a similarity matrix $S \in R^{Q \times Q}$. And similar to Eq. (3) and (4), we first obtain the refined node feature $\hat{x}_i$ based on the similarity matrix S. Then we concatenate the both raw node feature x_i and the refined node features $\widetilde{x}_i$ to get the relation-aware node feature $\hat{x}_i$. When using $\hat{x}_i$ to compute the contrastive loss, the impact of noise samples will be suppressed.

Selective Contrastive Learning

The proposed SCL is used for model updating, which is implemented via an external memory bank and a non-parametric loss. It mainly contains the following three parts:

Memory Bank Initialization (Dai et al. 2021). Assuming that the effective number of clusters in the current epoch is U, we store the cluster-level feature $\{v_{l_1}, v_{l_2}, \ldots, v_{l_U}\}$ in the memory bank $M^{Sel} \in R^{C \times U}$. And we use the averaged features of all instances in the cluster termed as $Mean(V_{l_i})$ to initialize M^{Sel}, where $Mean(\cdot)$ represents the average operation and V_{l_i} represents the feature set that contains all the instance feature vectors in cluster l_i.

Memory Updating. During training, there are $Q = P \times K$ query images in a mini-batch. In contrast to the previous memory updating methods (Xiao et al. 2017; Dai et al. 2021), which update all Q query instance features in the instance-level memory or select the hardest instance for each person to update the cluster feature, we choose Top-k hardest samples for each person to update M^{Sel}. Specifically, for a certain cluster l_i, we first rank the similarity order between the query q and cluster centroid $M^{Sel}[l_i]$. And then Top-k dissimilar query instances in a mini-batch will be selected to update the memory bank

$$M^{Sel}[l_i] \leftarrow \eta \cdot M^{Sel}[l_i] + (1 - \eta) \cdot q_{top_i}, i \in 1, \ldots, k \tag{6}$$

where $M^{Sel}[l_i]$ represents the updated feature centroid of class l_i, q_{top_i} is the Top-i dissimilar query instance with the class centroid and η is the momentum updating factor.

Selective Contrastive Loss. The proposed selective contrastive loss is defined by

$$L_{Scl} = -\sum_{k}^{n=1} log \frac{exp(M^{Sel}[l_i] \cdot q_{top_n}/\tau)}{\sum_{j=1}^{U} exp(M^{Sel}[l_j] \cdot q_{top_n}/\tau)} \tag{7}$$

where τ is a temperature factor. This loss achieves classification via pulling an instance close to the centroid of its class while pushing away from the centroids of all other classes. The entire loss for the model training is

$$L_{Total}(i) = L_{Scl}(x_i) + \lambda L_{Scl}(\hat{x}_i) \tag{8}$$

where λ is a balanced parameter and we set $\lambda = 0.5$.

Table 1: Comparison with SOTA methods on Market1501, DukeMTMC-reID and MSMT17.

methods	Market1501			DukeMTMC-reID			MSMT17		
	R1	R5	mAP	R1	R5	mAP	R1	R5	mAP
Unsupervised									
BUC (Lin et al. 2019)	66.2	79.6	38.3	47.4	62.6	27.5	–	–	–
SSL (Lin et al. 2020)	71.7	83.8	37.8	52.5	63.5	28.6	–	–	–
MMCL (Wang and Zhang 2020)	80.3	89.4	45.5	65.2	75.9	40.2	35.4	44.8	11.2
SCL (Pang et al. 2020)	82.2	89.9	54.4	69.9	79.7	47.2	41.4	53.6	13.3
IICS (Xuan and Zhang 2021)	89.5	95.2	72.9	80.0	89.0	64.4	56.4	68.8	26.9
RLCC (Zhang et al. 2021)	90.8	96.3	77.7	83.2	91.6	69.2	56.5	68.4	27.9
LUP-IDE (Fu et al. 2021)	91.0	–	77.9	82.2	–	65.9	68.9	–	39.8
CAP (Wang et al. 2021)	91.4	96.3	79.2	81.1	89.3	67.3	67.4	78.0	36.9
CC (Dai et al. 2021)	93.0	97.0	82.6	85.7	92.0	72.8	63.3	73.7	33.3
ICE (Chen, Lagadec, and Bremond 2021)	93.8	97.6	82.3	83.3	91.5	69.9	70.2	80.5	38.9
Ours	**94.8**	**98.2**	**87.5**	**87.6**	**94.3**	**77.0**	**74.2**	**85.4**	**49.0**
Supervised									
PCB (Sun et al. 2018)	93.8	97.5	81.6	83.3	90.5	69.2	68.2	–	40.4
ABDNet (Chen et al. 2019b)	95.6	–	88.3	89.0	–	78.6	82.3	–	60.8
FlipReID (Ni and Rahtu 2021)	95.3	–	88.5	89.4	–	79.8	83.3	–	64.3
AAformer (Zhu et al. 2021)	95.4	–	87.7	90.1	–	80.0	83.1	–	62.6

Experiments

Datasets and Evaluation Protocal

We evaluate our approach on three large-scale image-based person Re-ID datasets, *i.e*, Market-1501 (Zheng et al. 2015), DukeMTMC-reID (Ristani et al. 2016) and MSMT17 (Wei et al. 2018). We follow common practices and adopt the Cumulative Matching Characteristic (CMC) and mean Average Precision (mAP) to measure the performance.

Implementation Details

We use the ResNet-50 (He et al. 2016) pre-trained on ImageNet (Deng et al. 2009) as the backbone network. We remove the original classification layer and add GAP followed by batch normalization and L2 normalization layers, which will output 2048-dimensional features. For GCL, the number of images B in a graph is set to 16 and the number of temperature T is set to 5. At the beginning of each epoch, we compute Jaccard distance with K-reciprocal nearest neighbors (Zhong et al. 2017) and use DBSCAN (Ester et al. 1996) with a threshold of 0.6 for clustering, where K=30. For training, each image is resized to 256×128 and we adopt random flipping, padding, random cropping and random erasing (Zhong et al. 2020) for data augmentation. In each mini-batch, we sample 16 identities, each with 8 images. Thus, the number of images in a mini-batch are $16 \times 8 = 128$. We train our network for 60 epochs in total by the Adam optimizer (Kingma and Ba 2015). The initial learning rate is $3.5e-4$ and is divided by 10 at every 20 epochs. For contrastive loss, k is set to 2. The η and τ are set to 0.2 and 0.05, respectively.

Comparison with State-of-the-arts

We evaluate our approach on three image-based person Re-ID benchmarks and compare it with recent state-of-the-art methods. The detailed results summarized in Tab.1 show that our method achieves the best results on three large-scale datasets under the unsupervised setting. Specifically, on Market1501, we obtain the best performance among all the compared unsupervised methods with 94.8% in R1 and 87.5% in mAP. Compared with the currently best published method ICE (Chen, Lagadec, and Bremond 2021), we achieve 1.0% and 5.2% improvement on R1 accuracy and mAP, respectively. On DukeMTMC-reID, compared with the method CAP (Wang et al. 2021) that considers the camera variations during training, our method surpasses it by 6.5% and 12.7% in terms of R1 and mAP. On the challenging MSMT17, our method achieves an impressive 49.0% in mAP and 74.2% in R1, which outperforms CC (Dai et al. 2021) by 16.7% and 10.9% in terms of mAP and R1. The high performance indicates that our method can help to generate high-quality pseudo-labels and reduce the impact of clustering errors.

Compared with supervised methods including PCB (Sun et al. 2018), ABDNet (Chen et al. 2019b), FlipReID (Ni and Rahtu 2021) and AAformer (Zhu et al. 2021), our unsupervised method is still competitive. Although on the challenging MSMT17, the proposed method has a certain performance gap. Our unsupervised method achieves much better performance than the supervised PCB on three image-based person Re-ID benchmarks. The experimental results show the potential of unsupervised methods.

Ablation Studies

To verify the impact of each component, we conduct several experiments on DukeMTMC-reID and Market1501 datasets and show compared results in Tab.2. "SCL" means the proposed selective contrastive learning. "CR" means cluster refinement by GCL. "NS" means noise suppression. Without our components, the baseline model achieves poor results. The main reason is that the quality of pseudo-labels generated by unsupervised clustering is low, and the clustering results have a lot of noise. What's more, the training of the

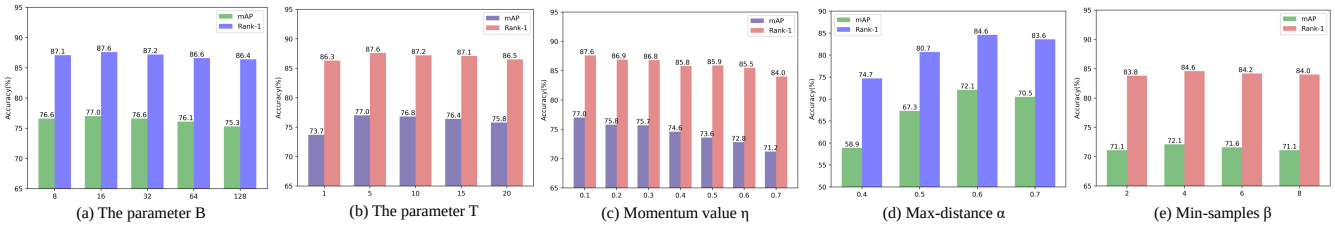

Figure 5: Illustration of (a) the impact of graph size B, (b) the impact of temperature T, (c) the impact of momentum updating factor, the impact of clustering hyper-parameters (d) the maximum distance between two samples, and (e) the minimum number of samples in a neighborhood.

Table 2: Comparison of different key components on DukeMTMC-reID and Market1501.

Model	Components			DukeMTMC-reID		Market1501	
	SCL	CR	NS	mAP	R1	mAP	R1
1	×	×	×	69.4	82.9	81.2	91.4
2	×	×	✓	70.6	83.7	82.1	92.1
3	✓	×	×	71.4	84.3	82.4	92.5
4	✓	×	✓	72.1	84.6	83.4	92.8
5	×	✓	✓	76.1	87.1	87.0	94.2
6	✓	✓	✓	77.0	87.6	87.5	94.8

Table 3: Comparison of different memory bank updating policies with the baseline method.

policy	DukeMTMC-reID			
	mAP	R1	R5	R10
Average	69.4	82.9	91.0	93.0
Random	68.6	82.1	90.1	92.5
$k = 1$	70.7	83.4	91.1	92.7
$k = 2$	71.4	84.3	91.6	93.4
$k = 4$	70.5	83.6	91.0	93.0

original contrastive loss is also affected by noise samples in a mini-batch. Thus, unreliable results are obtained.

The effectiveness of SCL. On DukeMTMC-reID and Market1501, compared with $Model1$, $Model3$ improves the R1 accuracy by 1.4% and 1.1%, respectively. A reasonable explanation for this improvement is that an appropriate strategy for updating the memory bank helps the network to learn a more discriminative representation.

The effectiveness of noise suppression. Compared with $Model1$, using GCL for noise suppression on DukeMTMC-reID and Market1501 brings 1.2% and 0.9% mAP gains respectively. On DukeMTMC-reID and Market1501, compared with $Model3$, using GCL for noise suppression improves the R1 accuracy from 84.3% and 92.5% to 84.6% and 92.8%, respectively. These results show that our GCL can reduce the impact of clustering errors.

The effectiveness of cluster refinement. As shown in $Model5$ and $Model6$, using GCL to refine the raw features before clustering improves the performance remarkably. On DukeMTMC-reID and Market1501, compared with $Model4$, $Model6$ improves the mAP from 72.1% and 83.4% to 77.0% and 87.5%, respectively. A reasonable explanation for this improvement is that the GCL can ensure the samples in a mini-batch learn from each other, which will potentially make the sample features with the same identity close to each other. Therefore, high-quality clustering results can be obtained by the refined sample features. It is worth noting that since the parameters of GCL need to be learned during the noise suppression process, we did not explore the situation where only using GCL before clustering.

The impact of the memory bank updating policy. As shown in Tab.3, we also explore the impact of different memory bank updating policies on DukeMTMC-reID. "Average" means that we average the feature of query instances of a special identity to update the corresponding centroid in the memory bank. "Random" means we randomly select a query instance. "$k = 1$" means we first rank the similarity order between the query instances and cluster centroid in the memory bank, and then select the Top-1 hardest query instance. Among above updating strategies, "$k = 2$" achieves the best performance. Compared with "$k = 1$", "$k = 2$" brings 0.9% R1 accuracy and 0.7% mAP gains respectively. The reason is that the hardest sample is often noisy in the unsupervised clustering. As a result, we choose "$k = 2$".

Sensitivity Analysis

We first analyze the impact of two hyper-parameters in the GCL module used for cluster refinement, *i.e.*, the number of nodes in a graph B and the temperature parameter T. We change the value of one parameter, while the other one is fixed during the experiments.

The impact of the hyper-parameter B. When using GCL to refine the raw features before clustering, we construct a series of small graphs in the order of the sorted dataset. Although samples with the same identity are gathered together after sorting, the number of person identity in each graph is random. In other words, changing the size of the graph will result in different numbers of identities. As a result, the size of the graph will affect the update of node features. As shown in Fig.5 (a), when B increases from 8 to 16, the R1 accuracy increases from 87.1% to 87.6% and mAP increases from 76.6% to 77.0%, respectively. When B gets larger, the Re-ID performance shows a slight drop. Thus, we set $B = 16$ in our experiments.

The impact of the hyper-parameter T. Comparing Fig.6 (a), (b), (c) and (d), we can find that the temperature parameter in Eq. (2) plays an important role in learning an effective relation distribution. Thus, we conduct experiments to investigate the impact of the hyper-parameter T on DukeMTMC-reID. As shown in Fig.5 (b), if the value of T is too large or too small, the network performance will decrease. As a result, we set $T = 5$ in our experiments.

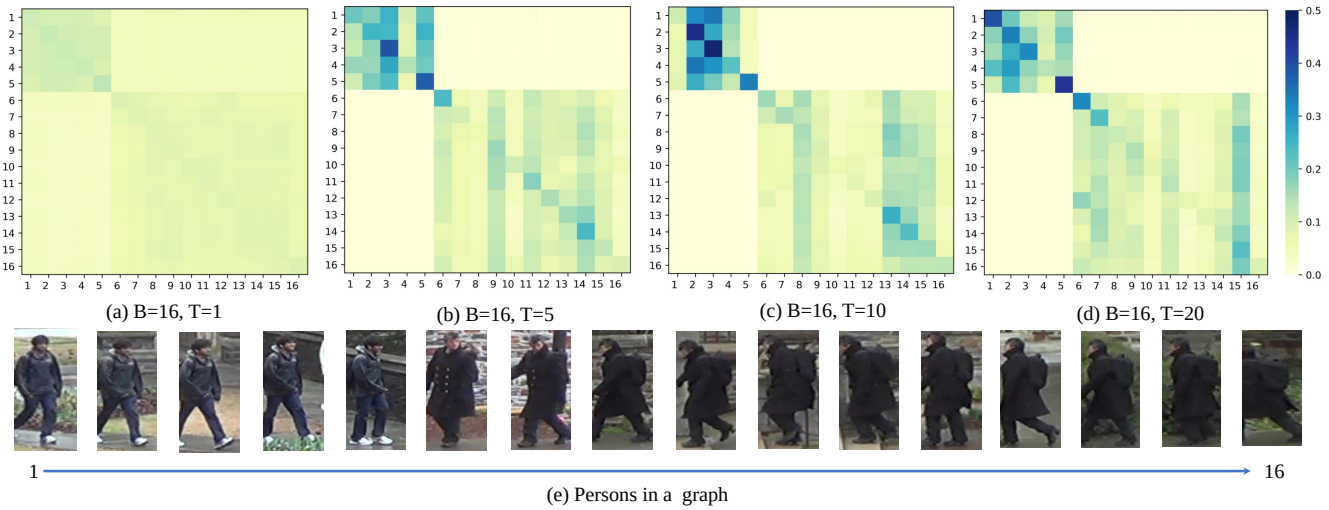

Figure 6: The attention scores learned in GCL before clustering.

The impact of the momentum updating factor. According to Eq.6, we use the momentum updating strategy to update the memory bank. And the momentum updating factor η controls the updating speed, which will affect the performance of the network. We conduct experiments to investigate its impact on DukeMTMC-reID. As shown in Fig. 5 (c), smaller η performs better than large. The smaller the value of η, the faster the memory bank update. We can conclude that smaller momentum updating factor benefits person Re-ID. As a result, we set η to 0.1 in our work.

The impact of clustering hyper-parameters. At the beginning of each epoch, we use DBSCAN (Ester et al. 1996) for clustering. The DBSCAN algorithm requires two hyper-parameters, the maximum distance between two samples α, and the minimum number of samples in a neighborhood β. We further analyze the impact of these two hyper-parameters. If the value of α is chosen too small, no points may become core points. In other words, all points will be marked as outliers. If it is chosen too large, the clusters will merge and most of the data points will be in the same clusters. To explore the impact of α, we use different values from 0.4 to 0.7 to train our method on DukeMTMC-reID. As shown in Fig. 5 (d), we can see that the value of α has a large impact on the results. And the best Rank-1 is 84.6% when $\alpha = 0.6$, so we set α to 0.6 in our work. On the other hand, if the value of β is chosen too large, it means that fewer points will become core points and more points will be marked as outliers. To explore the impact of β, we use different values from 2 to 8 to train our method on DukeMTMC-reID. As shown in Fig. 5 (e), we can see that the value of β will affect the performance of person Re-ID. And the best mAP is 72.1% when $\beta = 4$, so we set β to 4 in our work.

t-SNE visualization. To better understand the effect of the proposed GCL in improving the quality of the clustering, we conduct the t-SNE (van der Maaten and Hinton 2008) visualization experiments. Following (Yang et al. 2021), we randomly select 11 persons from Market1501 and visualize their features with t-SNE. In Fig. 7, we show the results of the model trained without or with GCL, respectively. We use different colors to denote person identities and different shapes to represent camera identities. Comparing Fig. 7 (a) and (b), we can find that the GCL indeed helps the network to learn a discriminative embedding space, in which the intra-class variance is minimized and the intra-class variance is maximized. And the intra-class features under different cameras are also well gathered. This verifies the advantage of our GCL in learning discriminative features. In addition, with the refined features by GCL, we can generate more accurate pseudo-label in the clustering step, which can further facilitate the optimization.

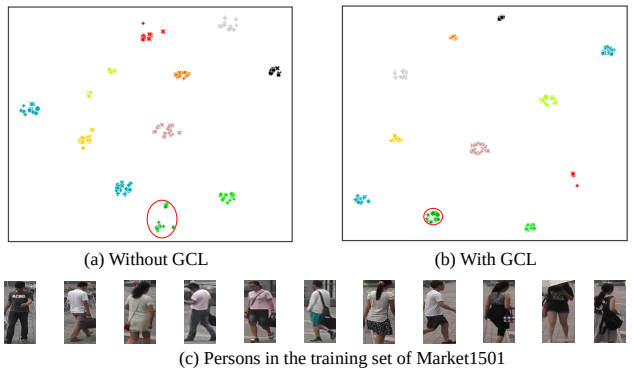

Figure 7: t-SNE visualization on the Market1501. Different colored dots represent different identities.

Conclusion

In this paper, we propose a novel adaptive clustering relationship modeling framework for unsupervised person Re-ID. Specifically, the relationship between unlabeled images is first explored by GCL and the refined features are then used for clustering to generate high-quality pseudo-labels. Considering that clustering errors are inevitable, GCL is also used to suppress noise in the mini-batch. In addition, we propose SCL to select Top-k hardest query features to update the cluster centroid in the memory bank, which is proved to be more informative and effective. Extensive experiments demonstrate that our method can outperform most methods on three benchmarks for unsupervised person Re-ID.

References

Chen, G.; Lu, J.; Yang, M.; and Zhou, J. 2019a. Spatial-temporal attention-aware learning for video-based person re-identification. *TIP*, 28(9): 4192–4205.

Chen, H.; Lagadec, B.; and Bremond, F. 2021. ICE: Inter-instance Contrastive Encoding for Unsupervised Person Re-identification. *arXiv preprint arXiv:2103.16364*.

Chen, T.; Ding, S.; Xie, J.; Yuan, Y.; Chen, W.; Yang, Y.; Ren, Z.; and Wang, Z. 2019b. Abd-net: Attentive but diverse person re-identification. In *ICCV*, 8351–8361.

Chen, T.; Kornblith, S.; Norouzi, M.; and Hinton, G. 2020. A simple framework for contrastive learning of visual representations. In *ICML*, 1597–1607.

Dai, Z.; Wang, G.; Yuan, W.; Zhu, S.; and Tan, P. 2021. Cluster Contrast for Unsupervised Person Re-Identification. *arXiv preprint arXiv:2103.11568*.

Deng, J.; Dong, W.; Socher, R.; Li, L.-J.; Li, K.; and Fei-Fei, L. 2009. Imagenet: A large-scale hierarchical image database. In *CVPR*, 248–255.

Deng, W.; Zheng, L.; Ye, Q.; Kang, G.; Yang, Y.; and Jiao, J. 2018. Image-image domain adaptation with preserved self-similarity and domain-dissimilarity for person re-identification. In *CVPR*, 994–1003.

Ester, M.; Kriegel, H.-P.; Sander, J.; Xu, X.; et al. 1996. A density-based algorithm for discovering clusters in large spatial databases with noise. In *KDD*, 226–231.

Fu, D.; Chen, D.; Bao, J.; Yang, H.; Yuan, L.; Zhang, L.; Li, H.; and Chen, D. 2021. Unsupervised Pre-training for Person Re-identification. In *CVPR*, 14750–14759.

Fu, Y.; Wei, Y.; Wang, G.; Zhou, Y.; Shi, H.; and Huang, T. S. 2019. Self-similarity grouping: A simple unsupervised cross domain adaptation approach for person re-identification. In *ICCV*, 6112–6121.

Ge, Y.; Zhu, F.; Chen, D.; Zhao, R.; and Li, H. 2020. Self-paced Contrastive Learning with Hybrid Memory for Domain Adaptive Object Re-ID. In *NIPS*, 11309–11321.

He, K.; Fan, H.; Wu, Y.; Xie, S.; and Girshick, R. 2020. Momentum contrast for unsupervised visual representation learning. In *CVPR*, 9729–9738.

He, K.; Zhang, X.; Ren, S.; and Sun, J. 2016. Deep residual learning for image recognition. In *CVPR*, 770–778.

Hermans, A.; Beyer, L.; and Leibe, B. 2017. In defense of the triplet loss for person re-identification. *arXiv:1703.07737*.

Ioffe, S.; and Szegedy, C. 2015. Batch normalization: Accelerating deep network training by reducing internal covariate shift. In *ICML*, 448–456.

Jin, X.; Lan, C.; Zeng, W.; and Chen, Z. 2020. Global distance-distributions separation for unsupervised person re-identification. In *ECCV*, 735–751.

Kingma, D. P.; and Ba, J. 2015. Adam: A method for stochastic optimization. In *ICLR*, 1–15.

Li, S.; Bak, S.; Carr, P.; and Wang, X. 2018. Diversity regularized spatiotemporal attention for video-based person re-identification. In *CVPR*, 369–378.

Lin, S.; Li, H.; Li, C.-T.; and Kot, A. C. 2018. Multi-task mid-level feature alignment network for unsupervised cross-dataset person re-identification. In *BMVC*.

Lin, Y.; Dong, X.; Zheng, L.; Yan, Y.; and Yang, Y. 2019. A bottom-up clustering approach to unsupervised person re-identification. In *AAAI*, 8738–8745.

Lin, Y.; Xie, L.; Wu, Y.; Yan, C.; and Tian, Q. 2020. Unsupervised person re-identification via softened similarity learning. In *CVPR*, 3390–3399.

Liu, K.; Ma, B.; Zhang, W.; and Huang, R. 2015. A spatio-temporal appearance representation for viceo-based pedestrian re-identification. In *ICCV*, 3810–3818.

Liu, X.; Zhang, P.; Yu, C.; Lu, H.; and Yang, X. 2021. Watching You: Global-guided Reciprocal Learning for Video-based Person Re-identification. In *CVPR*, 13334–13343.

Loy, C. C.; Xiang, T.; and Gong, S. 2009. Multi-camera activity correlation analysis. In *CVPR*, 1988–1995.

Ni, X.; and Rahtu, E. 2021. FlipReID: Closing the Gap Between Training and Inference in Person Re-Identification. In *EUVIP*, 1–6.

Pang, B.; Zhai, D.; Jiang, J.; and Liu, X. 2020. Unsupervised Constrative Person Re-identification. *arXiv preprint arXiv:2010.07608*.

Ristani, E.; Solera, F.; Zou, R.; Cucchiara, R.; and Tomasi, C. 2016. Performance measures and a data set for multi-target, multi-camera tracking. In *ECCV*, 17–35.

Sun, Y.; Zheng, L.; Yang, Y.; Tian, Q.; and Wang, S. 2018. Beyond part models: Person retrieval with refined part pooling (and a strong convolutional baseline). In *ECCV*, 480–496.

Tian, Y.; Sun, C.; Poole, B.; Krishnan, D.; Schmid, C.; and Isola, P. 2020. What makes for good views for contrastive learning. In *NIPS*, 6827–6839.

van der Maaten, L.; and Hinton, G. 2008. Visualizing Data using t-SNE. *JMLR*, 9: 2579–2605.

Wang, D.; and Zhang, S. 2020. Unsupervised person re-identification via multi-label classification. In *CVPR*, 10981–10990.

Wang, M.; Lai, B.; Huang, J.; Gong, X.; and Hua, X.-S. 2021. Camera-Aware Proxies for Unsupervised Person Re-Identification. In *AAAI*, 2764–2772.

Wang, X.; Han, X.; Huang, W.; Dong, D.; and Scott, M. R. 2019. Multi-similarity loss with general pair weighting for deep metric learning. In *CVPR*, 5022–5030.

Wei, L.; Zhang, S.; Gao, W.; and Tian, Q. 2018. Person transfer gan to bridge domain gap for person re-identification. In *CVPR*, 79–88.

Wu, H.; and Wang, X. 2021. Contrastive Learning of Image Representations with Cross-Video Cycle-Consistency. *arXiv preprint arXiv:2105.06463*.

Xiao, T.; Li, S.; Wang, B.; Lin, L.; and Wang, X. 2017. Joint detection and identification feature learning for person search. In *CVPR*, 3415–3424.

Xu, S.; Cheng, Y.; Gu, K.; Yang, Y.; Chang, S.; and Zhou, P. 2017. Jointly attentive spatial-temporal pooling networks for video-based person re-identification. In *ICCV*, 4733–4742.

Xuan, S.; and Zhang, S. 2021. Intra-Inter Camera Similarity for Unsupervised Person Re-Identification. In *CVPR*, 11926–11935.

Yan, B.; Wang, D.; Lu, H.; and Yang, X. 2020. Cooling-Shrinking Attack: Blinding the tracker with imperceptible noises. In *CVPR*, 990–999.

Yang, F.; Zhong, Z.; Luo, Z.; Cai, Y.; Lin, Y.; Li, S.; and Sebe, N. 2021. Joint Noise-Tolerant Learning and Meta Camera Shift Adaptation for Unsupervised Person Re-Identification. In *CVPR*, 4855–4864.

Yin, J.; Qiu, J.; Zhang, S.; Xie, J.; Ma, Z.; and Guo, J. 2021. Unsupervised Person Re-identification via Simultaneous Clustering and Consistency Learning. *arXiv preprint arXiv:2104.00202*.

Zhai, Y.; Lu, S.; Ye, Q.; Shan, X.; Chen, J.; Ji, R.; and Tian, Y. 2020. Ad-cluster: Augmented discriminative clustering for domain adaptive person re-identification. In *CVPR*, 9021–9030.

Zhang, X.; Ge, Y.; Qiao, Y.; and Li, H. 2021. Refining Pseudo Labels with Clustering Consensus over Generations for Unsupervised Object Re-identification. In *CVPR*, 3436–3445.

Zheng, L.; Shen, L.; Tian, L.; Wang, S.; Wang, J.; and Tian, Q. 2015. Scalable person re-identification: A benchmark. In *ICCV*, 1116–1124.

Zhong, Z.; Zheng, L.; Cao, D.; and Li, S. 2017. Re-ranking person re-identification with k-reciprocal encoding. In *CVPR*, 1318–1327.

Zhong, Z.; Zheng, L.; Kang, G.; Li, S.; and Yang, Y. 2020. Random erasing data augmentation. In *AAAI*, 13001–13008.

Zhu, K.; Guo, H.; Zhang, S.; Wang, Y.; Huang, G.; Qiao, H.; Liu, J.; Wang, J.; and Tang, M. 2021. AAformer: Auto-Aligned Transformer for Person Re-Identification. *arXiv preprint arXiv:2104.00921*.